Paper: ASAT-14-045-AE

14th International Conference on
***AEROSPACE SCIENCES & AVIATION TECHNOLOGY***,
***ASAT - 14*** – May 24 - 26, 2011, Email: asat@mtc.edu.eg
Military Technical College, Kobry Elkobbah, Cairo, Egypt
Tel: +(202) 24025292 –24036138, Fax: +(202) 22621908

# A Reverse Approach for Aerodynamic Analysis of a Typical UAV

M. A. M. Dafaalla*, M. Elhadi A. E.†

**Abstract:** A reverse approach has been followed to handle the problem of investigating the aerodynamic characteristics of a typical unmanned aerial vehicle model which are assumed unknown. Both numerical and experimental investigations have been conducted using wind tunnel and CFD facilities. The tests have been conducted in a low speed wind tunnel for a half section of real size tailless model. The aerodynamic loads have been measured and the loads were varied with pitch performed in range of (-2 to +26°) angles of attack with pre-selected test wind speeds between (25 – 40) m/s.
The test was carried out with different elevon deflection angles selected as (0-10-20-30°). The pressure tabs to investigate the chord-wise pressure distribution at Mean Aerodynamic Chord (MAC) for the sake of comparison between wind tunnel and CFD results. The test section conditions have been taken as inputs for the simulation with CFD Fluent software. Results revealed that the model was statically stable and the variation of aerodynamic coefficients to wind speed, angle of attack and elevon deflection is displayed. The pressure distribution along the MAC demonstrated the expected behaviour of the chord-wise pressure distribution during stall and laminar flow around the airfoil.

**Keywords:** Aerodynamic analysis, unmanned aerial vehicle, computational fluid dynamics, pressure distribution

## 1. Wind Tunnel Testing

### 1.1 Wind Tunnel Description

The low Speed Wind Tunnel is capable of delivering maximum airspeed of 80m/s (160 knots or 288km/hr) inside the test section. The test section size is 2.0m width × 1.5 m height × 5.8m length. The wind tunnel has an excellent flow quality (flow uniformity < 0.15%, temperature uniformity < 0.2°, flow angularity uniformity < 0.15°, turbulence < 0.06%), which is very important in aeronautical applications. With good flow quality and facility, it has the capability to deliver high accuracy and good repeatability of wind tunnel test results. The wind tunnel is furnished originally with three-strut support system for aircraft model installation .This type of model support system is commonly used in most well known wind tunnels for civil transport aircraft model testing (e.g. DNW Holland, NLR German, IAR-NRC Canada and ILST Indonesia).
The wind tunnel is equipped with a high accuracy 6-component balance to measure forces and moments in a 3-axis system which covers drag, side force, lift, roll, pitch and yaw (Fx, Fy, Fz, Mx, My and Mz), as shown in Fig. 1. The balance has a capability to measure all the static aerodynamic coefficients.

* MSc Student, Karary University, Khartoum-Sudan, amoya225@hotmail.com
† Assistant Professor, Karary University, mohadi20@hotmail.com

The aerodynamic coefficient can be tested as a function of angle of attack, sideslip, flap, elevator, aileron, rudder, trim-tab, etc. The balance is a pyramidal type with virtual balance moment at the centre of the test section. The aerodynamic loads can be tested at various wind directions by rotating the model via turntable. The accuracy of the balance is within 0.04% based on one standard deviation. The maximum load range is ±1200N for axial and side loads (i.e. drag force and side force).

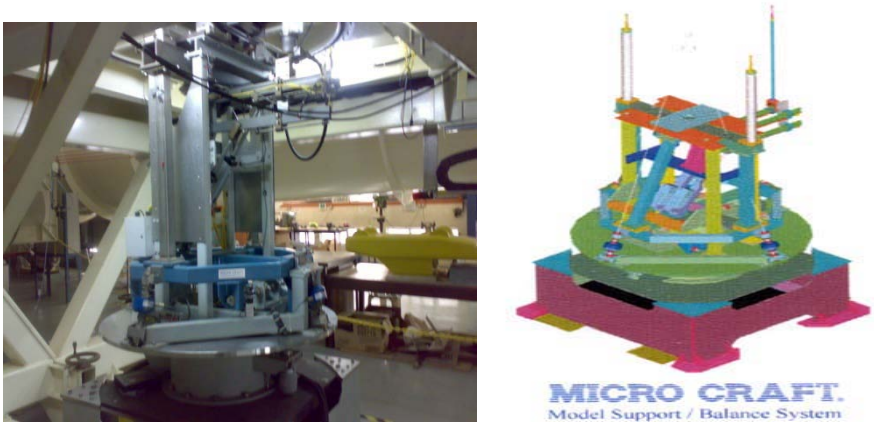


**Fig. 1 Wind tunnel Balance and Model Support System**

## 1.2 Model Description

The model has been made from fiber glass, carbon fiber and wood, in a real size dimensions (1.12m wing span, 1.95m length); See Fig. 2. A half model has been adopted to facilitate ease in test section. The model has been prepared with 20 drill orifices to install the pressure tabs for surface pressure measurements (12 at upper surface and 8 lower surfaces). The wing chord (MAC) is 0.675m and is located at 0.335m from the centre of fuselage.

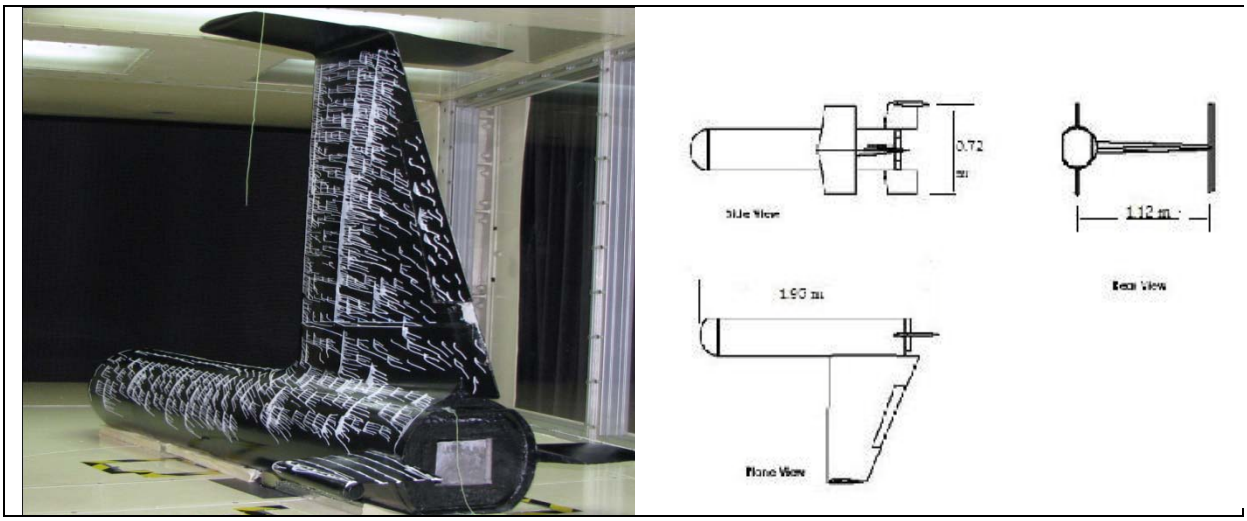


**Fig 2. Model Configuration**

**Model supporting and aligning in the test section**

The model is prepared and seated in the test section at zero degree in front of test section inlet (i: e the model longitudinal axis coincides with the X axis of test section); see Fig. 3.


**A desk to connect the model with 6-force component balance**


**Supporting points & pressure tabs passing point**

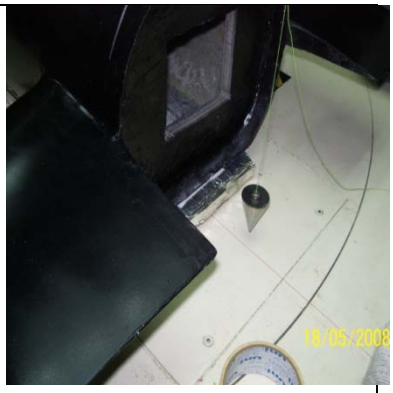

**Model aligning in the test section**

**Fig. 3 Model supporting and aligning**

## 1.3 Forces and Moments Measurements and Corrections

The semi span balance is a single piece that measures the five force components on a semi-span model. The balance measures drag force (Fx), normal force (Fz), pitching moment (My), yawing moment (Mz) and rolling moment (Mx). Balance moment centre (BMC) of the semi-span balance is the centre of the metric flange and is the origin of the coordinate system.

The result obtained from wind tunnel testing was corrected due to the blockage effect. The total blockage is mainly comprised of solid and wake blockage; see Fig 4.

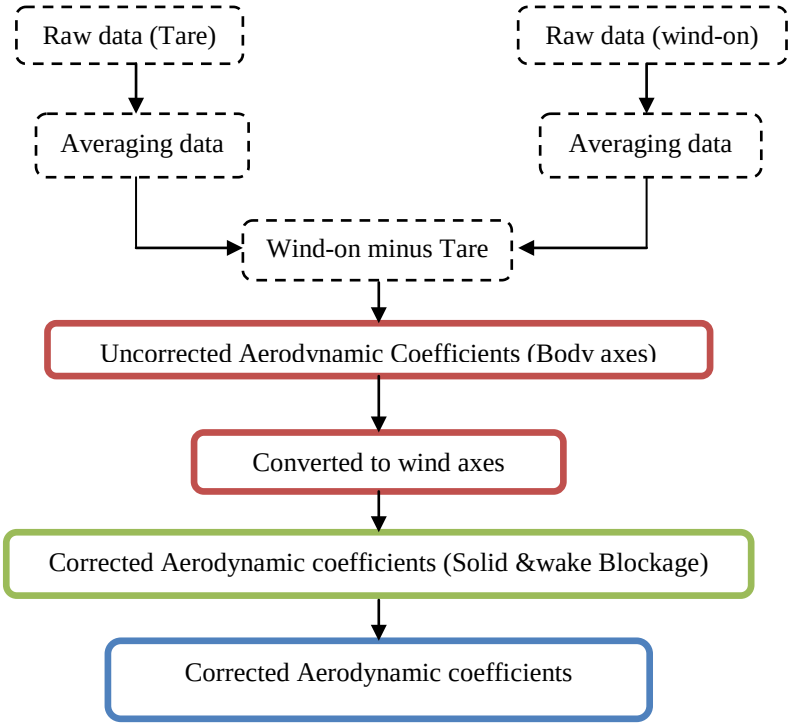


**Fig. 4 Force and moment data reduction flow chart**

### 1.4 Aerodynamic Forces and Moments Coefficients

Lift, drag, pitching moment and rolling moment coefficients could be calculated from raw data of a half UAV model testing while yawing moment could not be included in this phase. The results obtained from wind tunnel are acceptable compared to results of similar configurations, and the CFD simulation verified and ensured some of wind tunnel results. Plots for different parameters against angle of attack and wind speed are also displayed, see Figs. 5 - 7.

The tests are performed for the range of angles of attack from (-2 to 26°) at a wind speed 25m/s. However during the run a ($C_l$) increment from (-2 till 12°) angle of attack was observed. The peak of the curve is at 12°. Stall occurs at 15° angle of attack. However it is well known that for finite wings stall angles are usually less than for infinite ones (the present model is expected to stall at an angle less than 14°) .This is clear from Table (1). The lift curve slope of the aircraft is about 0.093 (a= 0.093deg$^{-1}$ (5.33rad$^{-1}$)) .The value of the lift curve slope is a typical value of an aircraft where the maximum lift coefficient ($C_{l\,max}$ ) is about 1.12. The aircraft has not shown a sudden stall but gentle drop of lift coefficient with lowest ($C_l$) of 0.97 at 20° angle of attack.

The increment of ($C_l$) for high angles (more than 12°) above the stall angle of attack may be due to fuselage effect which did not totally stall with the wing. The fuselage generated lift at all angles above 12°. The test section dimensions did not allow running for more than 26° angle of attack. Figure 7 shows the variation of drag coefficient with angle of attack. The zero lift drag ($C_D$°) was found to be around 0.057.

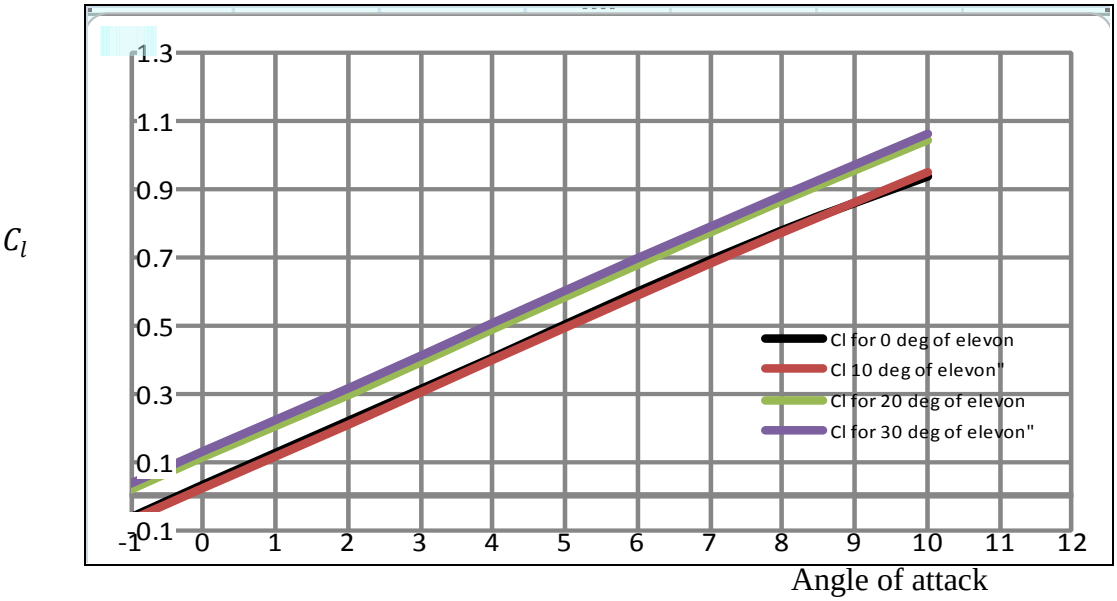


**Fig. 5 Lift coefficient for different elevon deflections; wind speed = 40m/s**

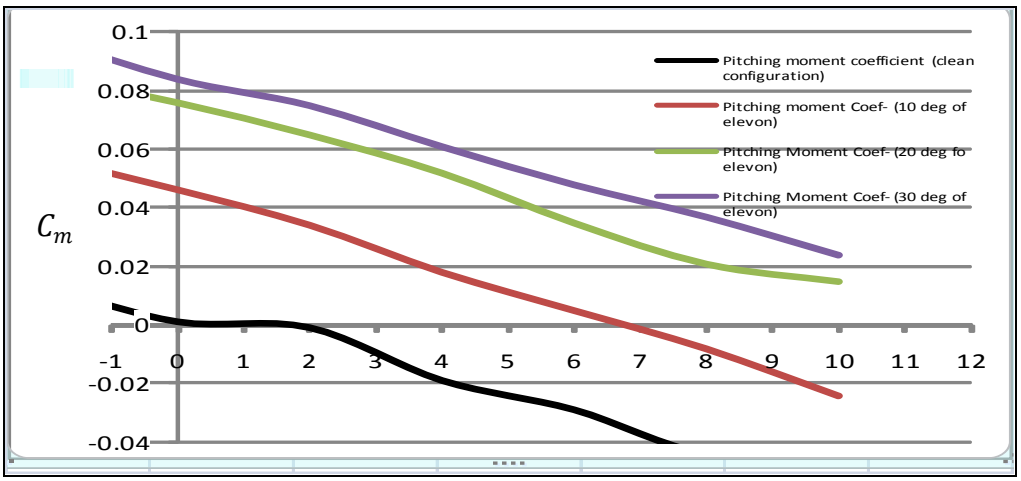


**Fig. 6 Pitching moment coefficient for different elevon deflections; wind speed = 40m/s**

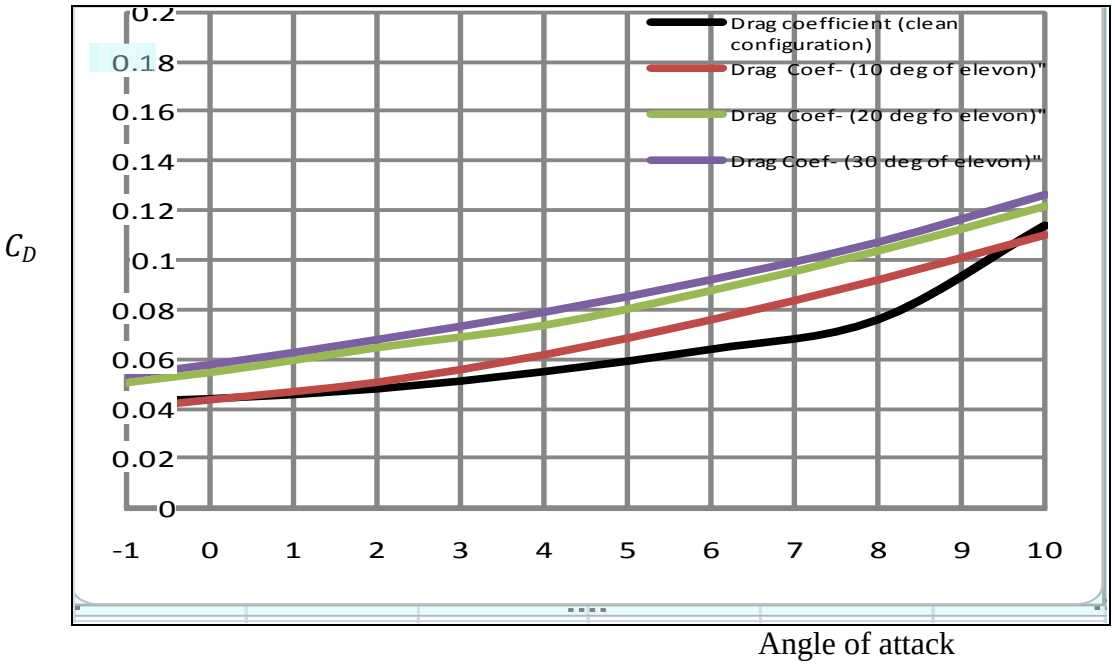


**Fig. 7 Drag coefficient for different elevon deflections; wind speed = 40m/s**

## 2. Pressure Distribution

The pressure coefficient is an important quantity. It leads directly to the value of lift coefficient. There are some preparations and arrangements of many components used to measure the pressure on the upper and lower surfaces of the wing on a specified section.

Pressure readings obtained experimentally were converted to pressure coefficient, Cp which is more significant for aerodynamic analysis. The pressure taping position as x/c points along the surface and the numbering of it corresponds to the scanivalve (SCV) port. The model has been prepared with 20 drill orifices to install the pressure tabs for surface pressure measurements; see Fig. 8. The wing chord is 0.675m and is located at 0.335m from the centre of fuselage. This is taken from a test at wind speed 25-40m/s for a clean configuration with angle of attack variations in the range between (-2 to 26°).

**Fig. 8 Pressure tabs installation**

The results of pressure measurements as plotted in Figs. 9 – 12 below. The stall phenomenon shows that pressure distribution has almost a constant value for high angles of attack.

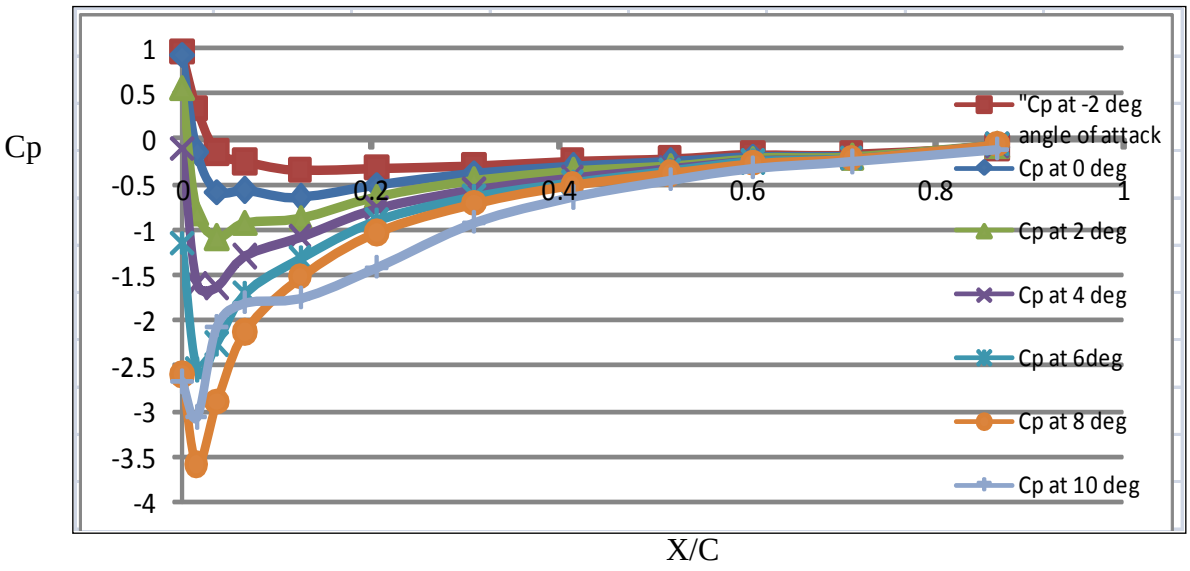


**Fig. 9 Upper surface pressure distribution at wind speed = 40 m/s**

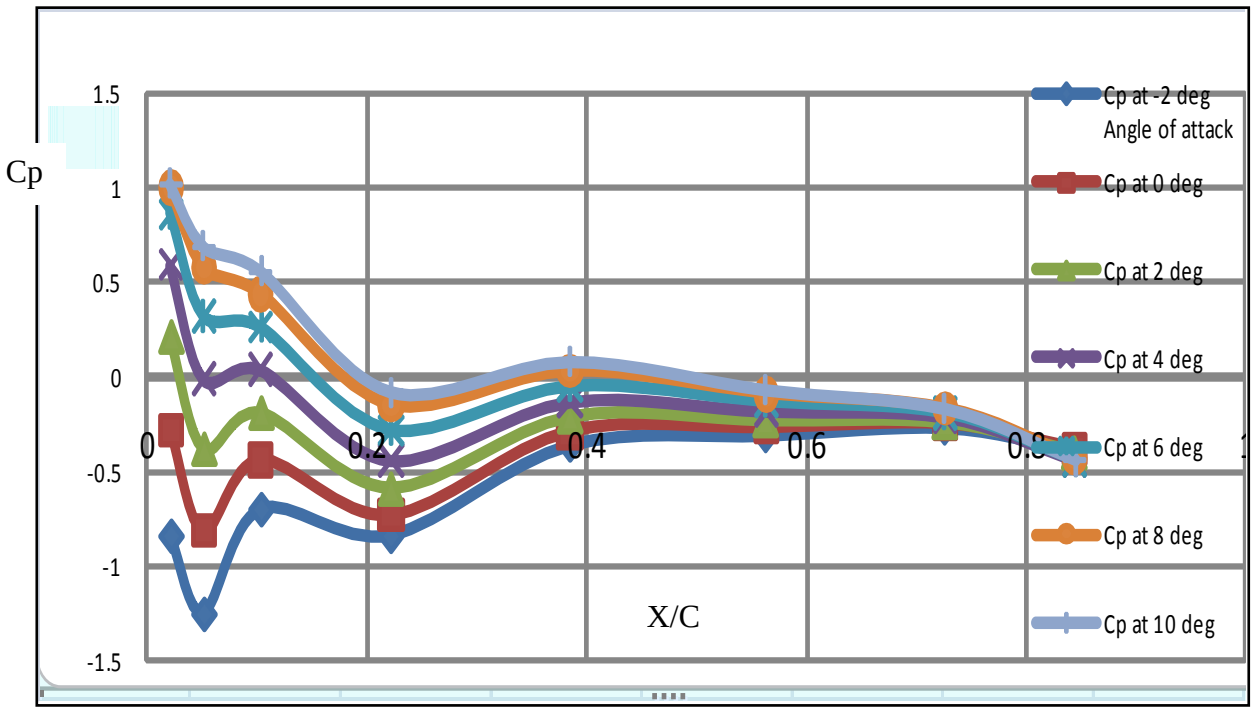


**Fig. 10 Lower surface pressure distribution at wind speed = 40 m/s**

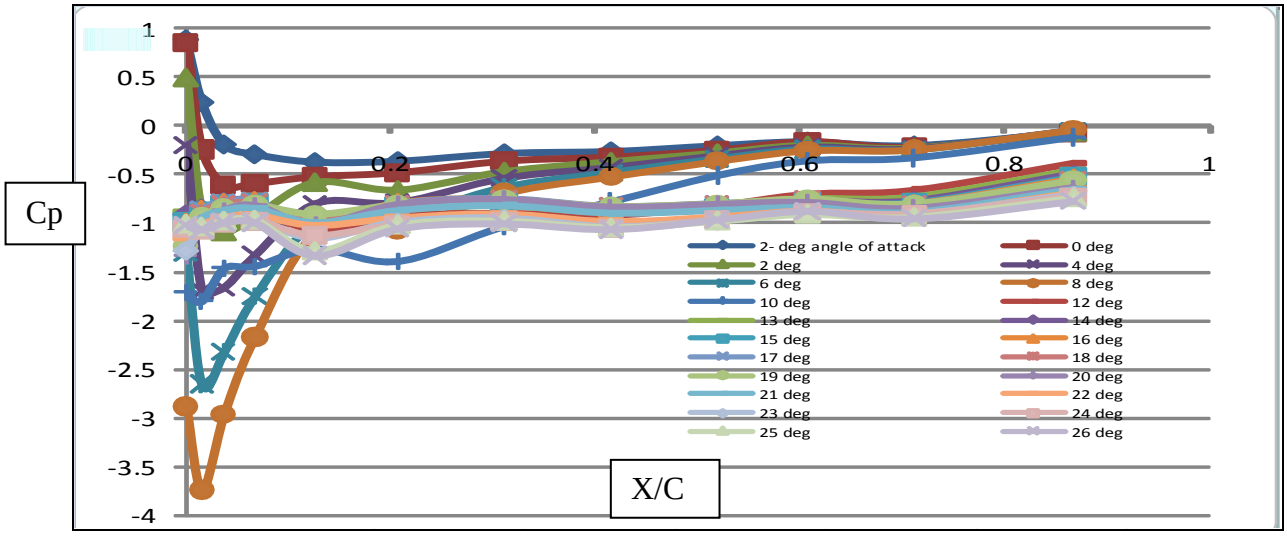


**Fig. 11 Upper surface pressure distribution at wind speed = 25 m/s**

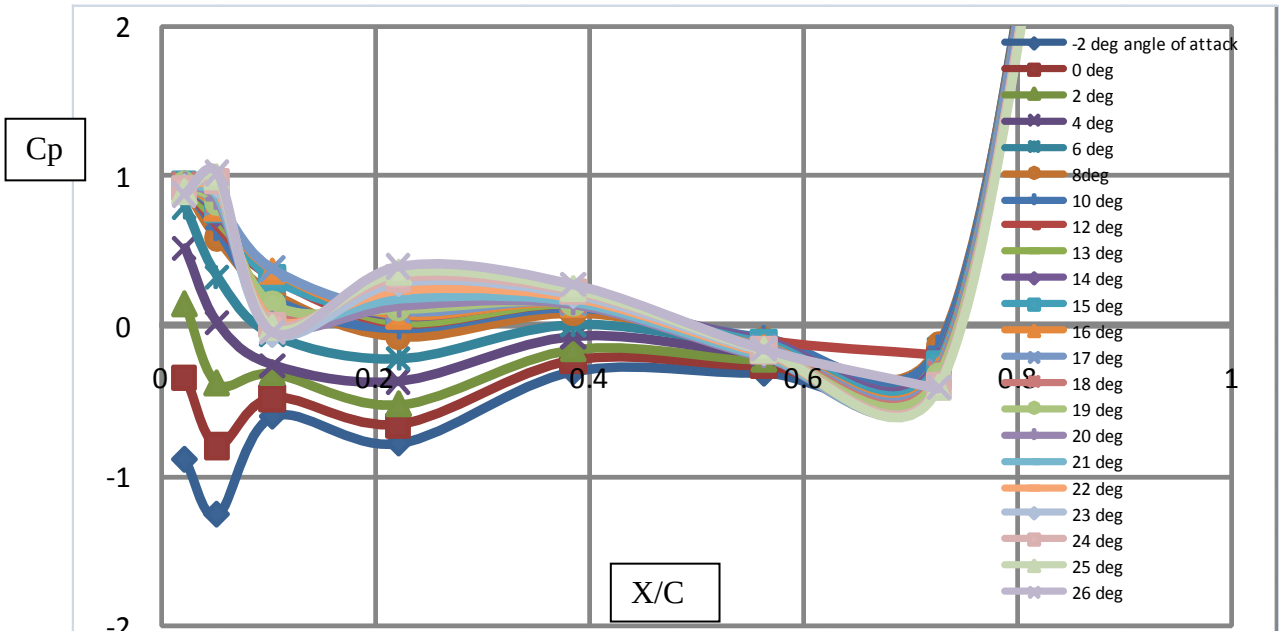


**Fig. 12 Lower surface pressure distribution at wind speed = 25 m/s**

## 3. Computational Fluid Dynamic Simulation

Computational Fluid Dynamics (CFD) is concerned with obtaining numerical solutions to fluid flow problems. The advent of high-speed and large-memory digital computers has enabled CFD to obtain solutions to many flow problems. Apart from the computer, the successes in modeling mathematical and physical problems and numerical methods have greatly advanced CFD simulations. The use of CFD software was successful in solving many complex flow problems with great accuracy.

A model was produced using CAD software (SOLID WORKS) with slight modification to two parts of the model in order to make it suitable for the work; see Fig. 13. The modification was necessary and it was believed to have little effect on the final results. The geometry was then meshed to the available computing resources of approximately 1.7 million nodes for all cases. For confirmation of grid independent solutions, the mesh size was doubled for one of the cases. Mesh arrangement was set up using mesh size function, and normally this method provides an acceptable mesh arrangement. A better mesh arrangement can be employed by meshing all the edges or by boundary layer method and these methods will require a much longer time. Meshes should be well designed to resolve important flow features which are dependent upon flow condition parameters (e.g., Re), such as the grid refinement inside the wall boundary layer.

### 3.1 Scope of Simulation

The Scope of Simulation Includes:

- CFD pre-processing using GAMBIT- which involves geometry, meshing, setting boundary zones and exporting mesh.
- Solver Processing in FLUENT– solver setting, setting boundary condition, initializing the domain and iterating for the solution.
- Post Processing – analyzing qualitative results such as contour and vector as well as producing qualitative output such as the force and pressure coefficient.
- Simulated results were then compared to the measured one of the wind tunnel testing.

- Preprocessing, simulating and post processing all the configurations. Table.4 shows the simulation setting and model configuration.
- Verification tests with different solution methods and checking for grid independent solution.
- A validation (i.e. solving the right equations) test was carried out by comparing simulated results to the measured wind tunnel test results for two different turbulence models.

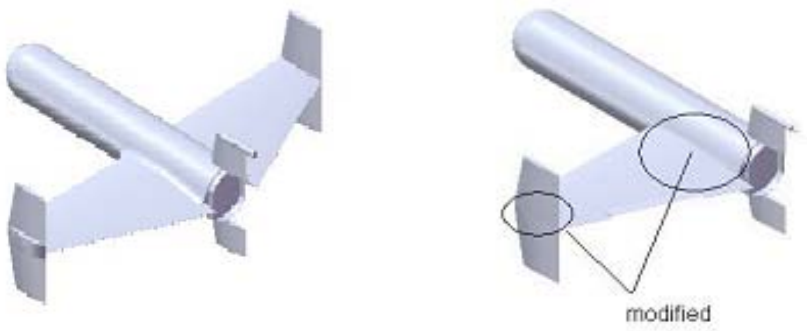


**Fig. 13 Slight modification to the model**

### 3.2 Pre-Processing

The solid model drawing of case study was subsequently used in the simulation on preprocessing using GAMBIT. The solid model was saved as ACIS file and was imported into GAMBIT. The activities done in preprocessing for GAMBIT are as follows:

1- Geometry Operations, Data Import and Geometry Cleanup
2- Edge and Face Meshing
3- Volume Meshing
4- Mesh Control –Size Functions, Using different type of Size Functions (Meshed, fixed, proximity and curvature)
5- Meshing Strategy and Quality, Mesh Generation and strategy to increase mesh quality
6- Boundary condition setting
7- Exporting and saving meshed files

In the preprocessing stage, the models geometry was processed and was meshed. In geometry process, the model was analyzed and flow domain was created. For case study in the wind tunnel, the flow domain was the same as the test section of the wind tunnel. For free stream simulation, the domain was chosen so that no effect of blockage was present as in the wind tunnel. The model was then meshed using automatic mesh generation available in GAMBIT. Size function was used to produce unstructured mesh. Although unstructured mesh is relatively easy to produce, the accuracy of this type of mesh especially in the boundary layer is slightly less. For flow where the friction drag is important, it is better to use structured mesh near the surface or to use the boundary layer placement. The structured mesh and the placement of boundary layer will take much longer time to produce. Using balance function, the model was meshed with a starting value of 8 and growth function of 1.2. This produced about 1.7 million cells. For a starting value of 6 and growth function of 1.2, the mesh size was 3 million cells. For automatic mesh generation, the mesh arrangement cannot be controlled and sometime area with high flow variables gradient did not get enough cells. The mesh quality was then analyzed and exported for simulation. It is recommended that work should be saved periodically through the process of making a mesh in Gambit because Gambit has a tendency to crash.

### 3.3 Simulating in FLUENT6.3

Further processing has to be carried in the solver such as:

- Setting up appropriate numerical parameters
- Choosing appropriate solvers and solution procedure
- Setting flow conditions e.g. inviscid, viscous, laminar, or turbulent, etc.
- Setting fluid properties e.g. density, viscosity, and thermal conductivity, etc.
- Selection of models e.g. type of turbulent model
- Setting Initial and Boundary Conditions

For the model in the wind tunnel, Velocity-inlet, Outflow/Pressure-outlet and Wall were used as boundaries. The boundary condition at the inlet was specified to be the same as the inlet condition of the wind tunnel test section. For the model in free stream flow, symmetry boundary condition was used for the symmetric plane. The inlet velocity of 40m/s was used, corresponding to a Reynolds number of $(1.63 \times 10^6)$. The flow is assumed to be incompressible with Mach number less than 0.6. Steady flow condition was assumed. Other input at inlet includes the density, viscosity and the turbulent boundary condition.

**Table.1.Simulation Modeling**

| Case | Configuration | α,[°] | δe,[°] | V∞,[m/s] | Mesh size | Turbulence model |
|---|---|---|---|---|---|---|
| 1 | δe= 0° , α= 0° | 0 | 0 | 40.03 | 1664482 | $k-\varepsilon$ |
| 2 | δe= 0° , α= 0° | 0 | 0 | 40.03 | 1664482 | Realizable $k-\varepsilon$ |
| 3 | δe= 0° , α= 4° | 4 | 0 | 39.93 | 1708397 | $k-\varepsilon$ |
| 4 | δe= 0° , α= 8° | 8 | 0 | 39.75 | 1698825 | $k-\varepsilon$ |
| 5 | δe= 0° , α= 10° | 10 | 0 | 39.53 | 1697448 | $k-\varepsilon$ |
| 6 | δe= 10° , α= 0° | 0 | 10 | 39.95 | 1676616 | $k-\varepsilon$ |
| 7 | δe= 20° , α= 0° | 0 | 20 | 40.03 | 1694338 | $k-\varepsilon$ |
| 8 | δe=30° , α= 0° | 0 | 30 | 40.03 | 1628764 | $k-\varepsilon$ |
| 9 | δe= 0° , α= 4° | 4 | 0 | 39.93 | 3292051 | $k-\varepsilon$ |
| 10 | Free stream flight | 0 | 0 | 70 | 1741777 | $k-\varepsilon$ |

where (δe= Elevon deflection angle, α= angle of attack)

### 3.3 CFD Results

Figures 14-16 show the CFD results of the velocity vector distribution and static pressure contours at some locations.

### Pressure coefficient distribution

The pressure coefficient distributions at upper surface are compared to the measured results of wind tunnel test results as shown in the figures below (Figs. 17-19). The comparisons are quite satisfactory. The simulation conditions were taken as the test section conditions (wind speed, density, dynamic pressure…..etc).

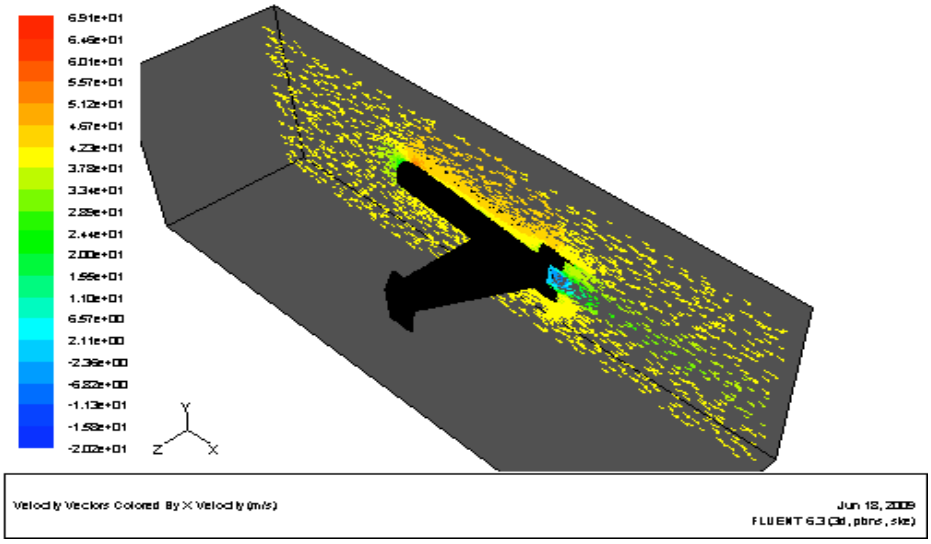


**Fig. 14 Velocity vector distribution at the centre of fuselage**

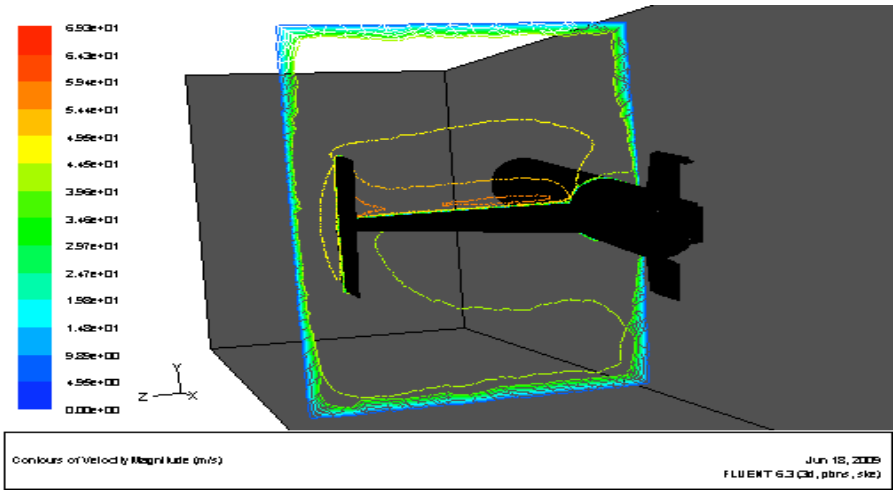


**Fig. 15 Velocity contour and vector distribution at the tip of the wing**

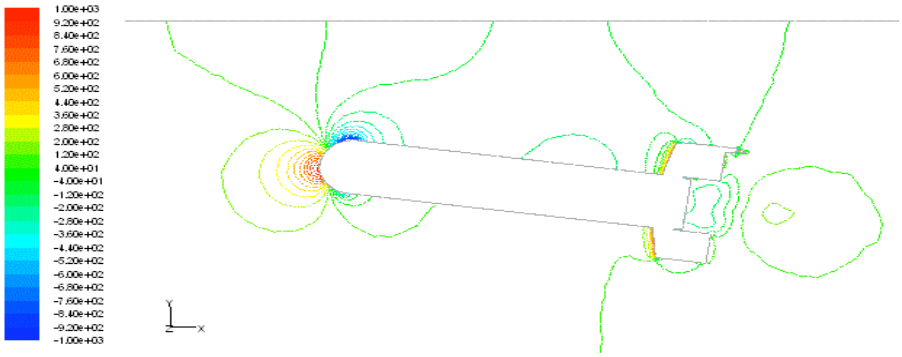


**Fig. 16 Static pressure contour α=8°**

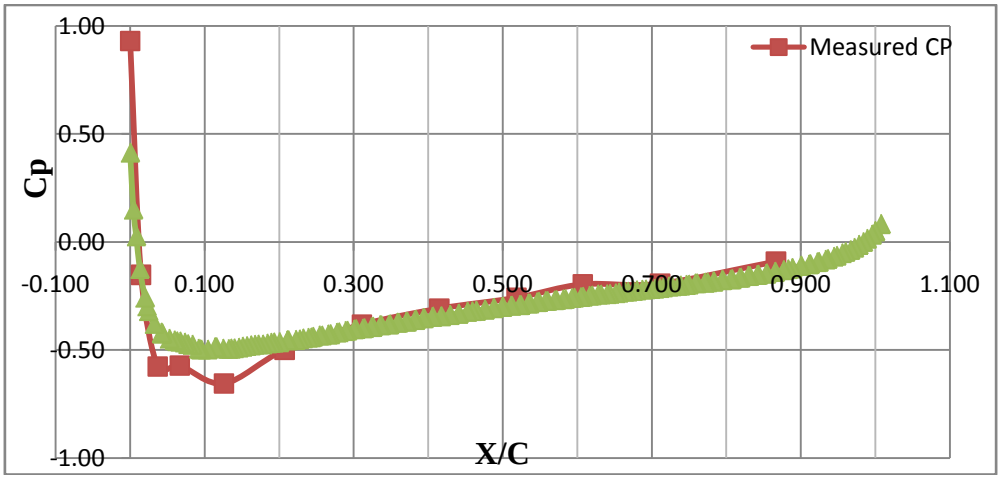


**Fig. 17 Upper surface pressure coefficient distribution at zero angle of attack**

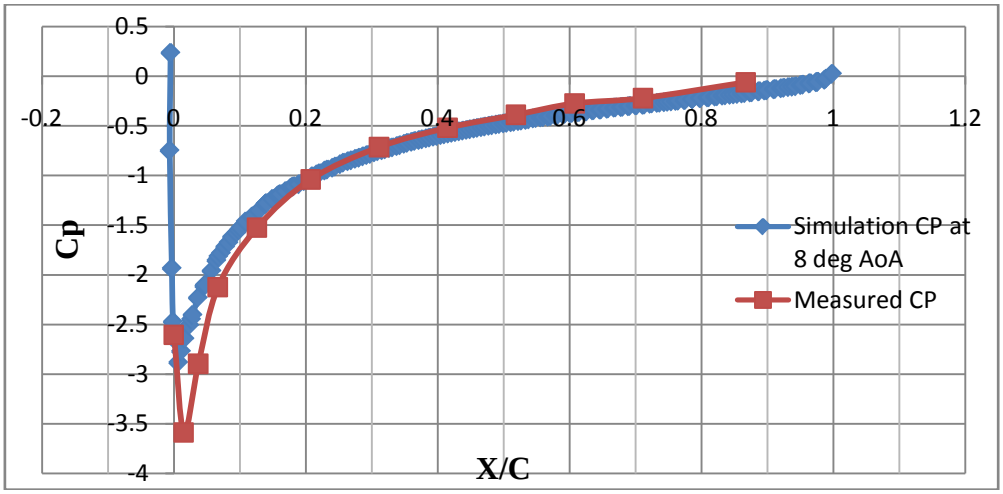


**Fig. 18 Lower surface pressure coefficient distribution at (8°) angle of attack**

## Lift and drag

The most common data required for most of the external flow aerodynamics are the forces and moments on the models. Figure 19 below indicates the simulated results of lift coefficient, ($C_l$) and drag coefficient, ($C_D$) for the model as compared to the measured results from wind tunnel testing. This is to compare the results from simulation with limited angle of attack for measured results. This verifies the measured results for lift coefficient and other aerodynamic coefficients. For drag coefficient a difference between measured and simulated results was observed. For drag force of model in the test section some factors affected the overall value of drag, also for simulation other factors affected the drag measurements .The reasons that may make a difference may be summarized as follows:

- The roughness of surface at wing and fuselage due to assembly affecting the frictional drag component for measured data.
- The control surfaces supporting may add more drag for model in test section.
- The supporting of model with test section floor may affect the results.
- The simulation software takes the case study as imported data; some of conditions and configuration differ from model tested in the wind tunnel.

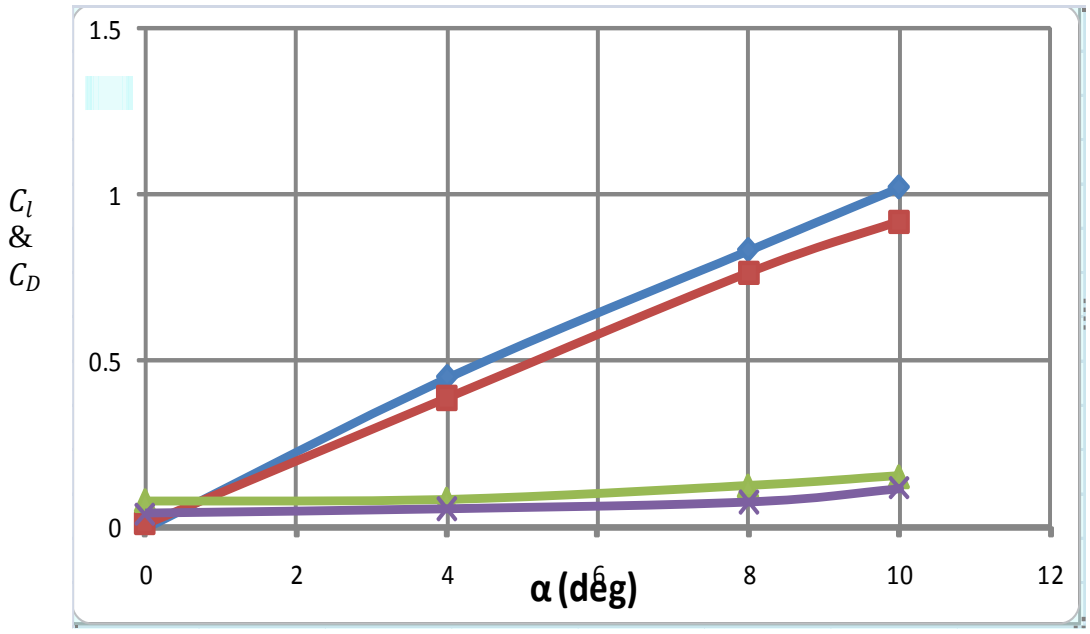


**Fig. 19 Comparison of simulated and measured coefficients**

## 4. References

[1] Barlow J.B. et al, "Low Speed Wind Tunnel Testing, 3rd edition, New York, A Wiley–Interscience Publication, 1999.

[2] Zan S.J., "Overview of Data Reduction Procedures for 3-D Aircraft Model Testing, In the Universiti Teknologi Malaysian Wind Tunnel, 2002.

[3] John A.D., "Computational Fluid Dynamics–The Basics with applications, New York, McGraw Hill Inc., 1995.